

A random matrix formulation of fidelity decay

T Gorin†‡, T Prosen§ and T H Seligman‡||

† Theoretische Quantendynamik, Albert-Ludwigs-Universität, Hermann-Herder-Str. 3, D-79104 Freiburg, Germany

‡ Centro Internacional de Ciencias, C.P. 62131 Cuernavaca, Morelos Mexico

§ Physics department, Faculty of Mathematics and Physics, University of Ljubljana, Jadranska 19, SI-1000 Ljubljana, Slovenia

|| Centro de Ciencias Fisicas, University of Mexico (UNAM), C.P. 62210 Cuernavaca, Morelos, Mexico

E-mail: thomas.gorin@physik.uni-freiburg.de

Abstract. We propose to study echo dynamics in a random matrix framework, where we assume that the perturbation is time independent, random and orthogonally invariant. This allows to use a basis in which the unperturbed Hamiltonian is diagonal and its properties are thus largely determined by its spectral statistics. We concentrate on the effect of spectral correlations usually associated to chaos and disregard secular variations in spectral density. We obtain analytic results for the fidelity decay in the linear response regime. To extend the domain of validity, we heuristically exponentiate the linear response result. The resulting expressions, exact in the perturbative limit, are accurate approximations in the transition region between the “Fermi golden rule” and the perturbative regimes, as exemplarily verified for a deterministic chaotic system. To sense the effect of spectral stiffness, we apply our model also to the extreme cases of random spectra and equidistant spectra. In our analytical approximations as well as in extensive Monte Carlo calculations, we find that fidelity decay is fastest for random spectra and slowest for equidistant ones, while the classical ensembles lie in between. We conclude that spectral stiffness systematically enhances fidelity.

PACS numbers: 05.45.Mt, 03.65.Yz

1. Introduction

Loschmidt echoes, proposed more than a century ago as a gedanken experiment [1], have been realized experimentally [2] measuring the corresponding auto correlation function known as *fidelity* [3]. Fidelity has also been used as the simplest benchmark for the reliability of quantum information devices [4], and recently Kaplan [5] has used fidelity of eigenstates to test uncertainty of quantisation. Many papers study general properties of fidelity under different regimes, including the semiclassical [6, 7], and the linear response regime [4, 8, 9]. The latter can be divided into the so called (standard) perturbative and the “Fermi golden rule” regimes [10]. In the perturbative regime, linear response theory will be correct for times long as compared to the Heisenberg time, while in the golden rule regime, it will break down before the Heisenberg time. The basic aim of this paper is to use a random perturbation V and, following the spirit of random matrix theory, to derive the universal features we may expect to be relevant for chaotic systems. The randomness of the perturbation implies orthogonal (or in the time reversal breaking case unitary) invariance. This in turn permits to use a basis in which the unperturbed Hamiltonian H_0 is diagonal. Then, only the spectral properties of H_0 enter the problem. We disregard secular variations in the spectral density and concentrate on fluctuations.

Our treatment shall make extensive use of linear response theory, because this will cover the basic needs of quantum information. Yet the model is not restricted to the lowest orders in this framework, and we shall see in Monte Carlo simulations how to extend heuristically our description to long time scales, exponentiating the linear response result. This will prove exact in the perturbative limit and will give good results even for moderately small perturbations. Note that in any case, we expect the linear response theory to hold much longer than the time corresponding to the inverse spectral span for which the eigenphases of the time evolution operator fill a small part of the unit circle, and which we call Zeno time. This regime allows for the straightforward expansion of the exponentials and thus is of limited interest. Furthermore in the context of information processing the linear response regime is most relevant, because in the semiclassical regime it will be almost impossible to have coherence in the quantum registers, and times short compared to the inverse spectral span are typically too short for quantum information processes.

We therefore construct the following model: H_0 is a diagonal matrix with an unfolded spectrum (constant level density) and V is a random matrix pertaining to the Gaussian orthogonal or unitary ensemble (GOE or GUE). To model chaotic systems we shall follow the quantum chaos conjecture [11], and use unfolded GOE or GUE spectra for H_0 . To contrast these with the possible extreme cases, we shall also consider picket-fence (equally spaced) and random spectra. Actually, any spectrum can be used, whose form factor is known. Random spectra are often associated with integrable systems [12], but we must keep in mind that the effects we describe in echo-dynamics are state dependent, and thus other important properties of integrable systems such as invariant tori will typically also be relevant. We can therefore expect the GOE and the GUE

cases to relate directly to chaotic systems, and indeed we shall see that such a relation can be established, as shown in [13]. Indeed, the random matrix model used there, is very similar to the one we propose. Note that the use of a random perturbation has been proposed in reference [4].

The other important aspect in echo dynamics is the dependence on the initial state. The analysis of coherent states – so important in other studies – is not considered here, because, typically, we do not expect to have an underlying classical model at our disposal. The most important property is then the spectral span of the initial state. We shall mainly consider two extremes: the evolution of an eigenstate of the unperturbed system, and the evolution of a random state with a given, but fairly large spectral span. The latter is the relevant case for quantum computing. This is easily understood if we think *e.g.* of Fourier transforms. The transforms of simple functions such as Gaussians are readily done analytically, while we would like to exploit the quantum algorithm for an arbitrarily complicated case. Yet it is also interesting to consider eigenfunctions partially because of the applications in the context of effects of different types of quantisation [5] but also because these display most markedly the effects of spectral fluctuations.

We measure the distortion of a state by calculating the fidelity, which may be interpreted as the autocorrelation function of a forward evolution with H_0 and a time reversed evolution with the perturbed Hamiltonian $H = H_0 + \lambda V$. The same quantity can also be interpreted as a cross correlation function of the same initial state evolving under the two Hamiltonians H_0 and H . Specifically, if $\Psi(t)$ and $\Psi_0(t)$ are the functions evolving under H and H_0 , respectively, from the same initial function $\Psi(0) = \Psi_0(0)$, we define the *fidelity amplitude* as the matrix element

$$f(t) = \langle \Psi_0(t) | \Psi(t) \rangle = \langle \Psi(0) | U_0(-t) U(t) | \Psi(0) \rangle , \quad (1)$$

where $U_0(t)$ is the unitary propagator associated with H_0 , and $U(t)$ is the one associated with H . From the point of view of a quantum Loschmidt echo, $U_0(-t) U(t)$ would be the “echo”-operator. The fidelity is usually defined as $F(t) = |f(t)|^2$. In the interaction picture with the state of the system denoted by $x(t)$, the fidelity is simply the autocorrelation function. To see this we recall that

$$\Psi(t) = U_0(t) x(t) \Rightarrow i\hbar \partial_t x(t) = \lambda \tilde{V}(t) x(t) , \quad (2)$$

where $\tilde{V}(t) = U_0(-t) V U_0(t)$. Hence:

$$f(t) = \langle x(0) | U_0(-t) | \Psi(t) \rangle = \langle x(0) | x(t) \rangle . \quad (3)$$

In the next section we recall the relevant linear response relations in the interaction picture, and apply them to the calculation of the fidelity amplitude. In the perturbative regime, *i.e.* for small λ , the Born series can be summed to yield the well known Gaussian decay. We therefore give a phenomenological formula for the general case by simply exponentiating the linear response result, and we compare to Monte Carlo simulations to establish the accuracy of this formula. In section 2.5, we apply our results to the standard map, using calculations by Cerruti and Tomsovic [13]. We find that our

heuristic formula is not only simpler, but also closer to the numerical experiment than the expression derived there.

In section 3, we proceed to calculate the fidelity. We observe a marked difference between the behaviour of a single eigenstate and that of a superposition. In the former case, the differences resulting from different spectral statistics are enhanced. Again we compare with numerical calculations. In section 4 we study the asymptotic behaviour of the fidelity for long times in various situations, and we obtain some analytical results from the perturbation theory. All these studies use spectral correlation functions in the large N limit for the GOE (and GUE) case. Finally we give some concluding remarks in section 5.

2. Fidelity amplitude

In this section we shall first derive a linear response formula for the decay of the fidelity amplitude. The central quantity of interest is here the correlation integral, which is a double integral over the autocorrelation function of the perturbation in the interaction picture. Given that the perturbation is taken from the GOE (GUE), the correlation integral only depends on the spectral properties of H_0 , and we shall evaluate the correlation integral for different cases. Note that, unless stated otherwise, GOE perturbations are used throughout this article. We then discuss the possibility to extend the validity of the linear response result by packing it into an exponential. This phenomenological formula works very well up to the crossover between the perturbative and the Fermi golden rule regime. In the last part of this section we discuss the sample fluctuations of the fidelity amplitude concentrating on the regime of high fidelity, as this is the one most relevant for quantum information applications.

As a preliminary step, let us introduce more convenient units for time and energy. In order to take advantage of the orthogonal (unitary) invariance of the perturbation, we write the Schrödinger equation in the eigenbasis of H_0 :

$$H_0 = \text{diag}(\overset{\circ}{E}_\alpha), \quad U_0(t) = \text{diag}(e^{-i\overset{\circ}{E}_\alpha t/\hbar}). \quad (4)$$

Thus, we obtain in the interaction picture:

$$i\hbar \partial_t x(t) = \lambda \text{diag}(e^{i\overset{\circ}{E}_\alpha t/\hbar}) V \text{diag}(e^{-i\overset{\circ}{E}_\beta t/\hbar}) x(t). \quad (5)$$

Denoting with d the average level spacing in the spectrum of H_0 (for simplicity we shall assume that d is constant in the energy range of interest), the Heisenberg time is defined as $t_H = 2\pi\hbar/d$. It is convenient to measure time in units of t_H and energy in units of d , introducing the dimensionless time $s = t/t_H$ and spectrum $\{\overset{\circ}{e}_\alpha = \overset{\circ}{E}_\alpha/d\}$. Then we obtain for $x'(s) = x(t_H s)$:

$$i \partial_s x'(s) = \frac{2\pi\lambda}{d} \text{diag}(e^{2\pi i \overset{\circ}{e}_\alpha s}) V \text{diag}(e^{-2\pi i \overset{\circ}{e}_\beta s}) x'(s). \quad (6)$$

This shows, that without restriction of generality, we may assume that the Heisenberg time and the average level spacing are both equal to one – and in the rest of the paper

we shall indeed do so. This allows us to stick to the symbols for time and energy, as introduced in the beginning.

2.1. Linear response

With $U_0(t) = \text{diag}[\exp(-2\pi i \mathring{E}_\alpha t)]$, and the shorthand $\tilde{V}(t) = U_0(-t) V U_0(t)$, we can approximate $x(t)$ using the Born series:

$$x^{(n)}(t) = x(0) - 2\pi i \lambda \int_0^t d\tau \tilde{V}(\tau) x^{(n-1)}(\tau), \quad x^{(0)}(t) = x(0). \quad (7)$$

Up to second order we obtain: $x^{(2)}(t) = X(t) x(0)$, where

$$X(t) = 1 - 2\pi i \lambda \int_0^t d\tau \tilde{V}(\tau) - 4\pi^2 \lambda^2 \int_0^t d\tau \int_0^\tau d\tau' \tilde{V}(\tau) \tilde{V}(\tau'). \quad (8)$$

Note that $X(t)$ is the linear response approximation of the echo operator, mentioned above. In general, we are interested in the various moments of the components of $x^{(2)}(t)$. Their knowledge will allow us to calculate averages of the fidelity, as well as the survival probability or even the purity. However, we may additionally choose the initial state $x(0)$ to be random and eventually even H_0 could be a member of some ensemble. In particular, if we want to keep the initial states arbitrary, it is more convenient to consider the various moments of the matrix elements $X_{\alpha\beta}(t)$, when the average is performed over the GOE (or GUE) matrix V . We define these matrix ensembles such that

$$\langle V_{ij} V_{kl} \rangle = \begin{cases} \delta_{il} \delta_{jk} & : \text{GUE} \\ \delta_{ik} \delta_{jl} + \delta_{il} \delta_{jk} & : \text{GOE} \end{cases}. \quad (9)$$

Our linear response approach is very similar to the one by Prosen and coworkers [14]. However, in their work, H_0 and V are fixed while the average is taken over initial conditions only. Here we will primarily average over the perturbation V , thereafter over H_0 , if we consider an ensemble, and finally over initial states, if these are random.

The spectral correlation function In order to average the linear response operator $X(t)$, given in (8), we basically need the correlation function: $\langle \tilde{V}(\tau) \tilde{V}(\tau') \rangle_V$, where $\langle \dots \rangle_V$ denotes the ensemble average over the random matrix V . Here, we present the full calculation for the GOE perturbation, only. With $\Delta_\alpha(t) = \exp(-2\pi i \mathring{E}_\alpha t)$, we obtain:

$$\begin{aligned} \langle [\tilde{V}(\tau) \tilde{V}(\tau')]_{\alpha\beta} \rangle_V &= \sum_\gamma \Delta_\alpha(-\tau) \langle V_{\alpha\gamma} \Delta_\gamma(\tau - \tau') V_{\gamma\beta} \rangle_V \Delta_\beta(\tau') \\ &= \sum_\gamma \Delta_\alpha(-\tau) \Delta_\gamma(\tau - \tau') \Delta_\beta(\tau') [\delta_{\alpha\gamma} \delta_{\gamma\beta} + \delta_{\alpha\beta}] \\ &= \delta_{\alpha\beta} C_\alpha(\tau' - \tau), \quad C_\alpha(t) = 1 + \sum_\gamma e^{2\pi i (\mathring{E}_\gamma - \mathring{E}_\alpha) t}. \end{aligned} \quad (10)$$

The correlation function (10) can be expressed in terms of the two-point form factor $b_2(t)$, one of the important fluctuation measures in quantum chaos studies [15]. Namely, if we denote with $\langle \dots \rangle_0$ the average over the diagonal matrix H_0 , we may write:

$$\langle C_\alpha(t) \rangle_0 = 2 + \delta(t) - b_2(t). \quad (11)$$

The H_0 -average makes sure to obtain a well behaved, *i.e.* smooth, two-point form factor. Though, note that in practice, this additional averaging may be avoidable. The corresponding expression for the GUE perturbation is: $1 + \delta(t) - b_2(t)$.

Let us now turn to the calculation of the average echo operator in the linear response approximation:

$$\langle X_{\alpha\beta}(t) \rangle_V = \delta_{\alpha\beta} - 4\pi^2 \lambda^2 \int_0^t d\tau \int_0^\tau d\tau' \delta_{\alpha\beta} C_\alpha(\tau'). \quad (12)$$

Additional averaging over H_0 gives a scalar result:

$$\langle \langle X_{\alpha\beta}(t) \rangle_V \rangle_0 = 1 - 4\pi^2 \lambda^2 \mathcal{C}(t), \quad (13)$$

where

$$\mathcal{C}(t) = t^2 + t/2 - \int_0^t d\tau \int_0^\tau d\tau' b_2(\tau'). \quad (14)$$

Note that the integration of the delta function gives $\frac{1}{2}$. For the GUE perturbation, the t^2 -term should be cut in half. Due to the scalar result in equation (13), the average fidelity amplitude does not depend on the initial state:

$$\langle \langle f(t) \rangle_V \rangle_0 = \langle \langle \langle X(t) \rangle_V \rangle_{\overset{\circ}{x}} \rangle_0 = 1 - 4\pi^2 \lambda^2 \mathcal{C}(t). \quad (15)$$

Here $\langle \dots \rangle_{\overset{\circ}{x}}$ is a short hand for the expectation value with respect to the initial state. If we avoid averaging over H_0 , the average fidelity amplitude reads:

$$\langle f(t) \rangle_V = \langle \langle X(t) \rangle_{\overset{\circ}{x}} \rangle_V = 1 - 4\pi^2 \lambda^2 \int_0^t d\tau \int_0^\tau d\tau' \sum_\alpha |\overset{\circ}{x}_\alpha|^2 C_\alpha(\tau'). \quad (16)$$

If the participation ratio of the initial state $\overset{\circ}{x}$ is sufficiently large, *i.e.* if the inverse participation ratio, $\text{ipr}(\overset{\circ}{x}) = \sum_\alpha |\overset{\circ}{x}_\alpha|^4$, is sufficiently small, this may lead to self-averaging – just as it does for the autocorrelation function of certain deterministic systems. Then we may still use the general result, equation (15), inserting the proper two-point form factor for this case.

2.2. Correlation integral

Clearly, the correlation integral $\mathcal{C}(t)$ is the essential quantity which determines the fidelity (amplitude) decay. It is shown in figure 1 for the Poisson, GOE, GUE, and picket-fence spectrum. The two-point form factor $b_2(t)$ is zero in the Poisson case, while for all other cases, it is given in Appendix A. The level repulsion, present in all but the first spectrum, tends to slow down the increase of the correlation integral. This is simply a consequence of the so called “correlation hole” [16], which can be found in the integrand of equation (13). Note however that for large times the quadratic increase with time remains essentially unaffected [panel (a)]. In figure 1(b), we subtract the t^2 -term in order to display more clearly the particular effects of the different spectral correlations. While in the Poisson case the remaining term is linear, in the correlated

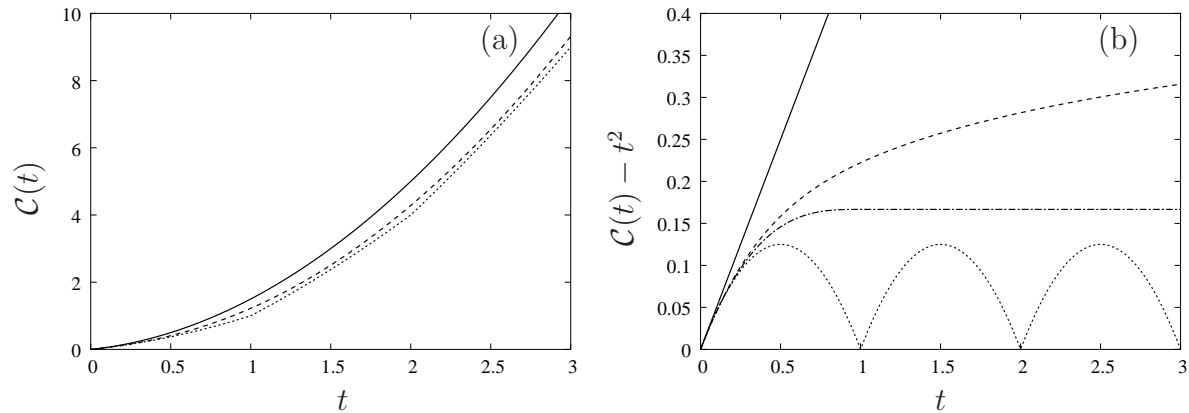


Figure 1. (a) The correlation integral $\mathcal{C}(t)$, equation (14), for the Poisson spectrum (solid line), the GOE spectrum (dashed line), and the picket-fence spectrum (dotted line). (b) The function $\mathcal{C}(t) - t^2$, for the three spectra in panel (a), and for the GUE spectrum (dash-dotted line).

spectra (GOE, GUE and picket-fence) the linear increase at the origin is capped. In fact, we can calculate explicitly the asymptotic behaviour of the correlation integral. In the GOE case, using the exact formula (A.11), we obtain:

$$\mathcal{C}(t) = t^2 + \frac{t}{2} - \int_0^t d\tau B(\tau) = t^2 + \frac{\ln t + 2 + \ln 2}{12} + O(t^{-1}). \quad (17)$$

In the picket-fence case, the correlation integral (with the t^2 term subtracted) has zeros at integer values of t . The GUE spectrum leads to $\mathcal{C}(t) - t^2$ approaching $2\pi^2/3$ from below.

2.3. Exponentiated linear response

In the perturbative regime, *i.e.* in the limit of small λ , the fidelity decay is known to be Gaussian [3]. This can readily be reproduced in the present context. The Born series can be trivially summed under the assumption that eigenstates are not affected by the perturbation. The result corresponds to the exponentiation of equation (15):

$$\langle f(t) \rangle = \exp[-4\pi^2 \lambda^2 \mathcal{C}(t)]. \quad (18)$$

This result is exact in the limit $2\pi\lambda \ll 1$, only, but we shall show below that errors are fairly small even for $\lambda \sim 0.1$, and negligible for $\lambda \sim 0.01$. The essential point is that the correlation integral, whether used in equation (15) or (18) clearly displays the transition between a linear decay at short times and a quadratic decay at long times. Accordingly, for small λ , the decay of the fidelity amplitude is dominantly Gaussian, whereas for larger λ , it is dominantly exponential [7, 8].

Figure 2 shows the behaviour of the fidelity amplitude according to equation (18) for the GOE and the Poisson case, in the large N limit. For the latter, the linear and quadratic terms are also shown separately. Note that the GOE results lie systematically

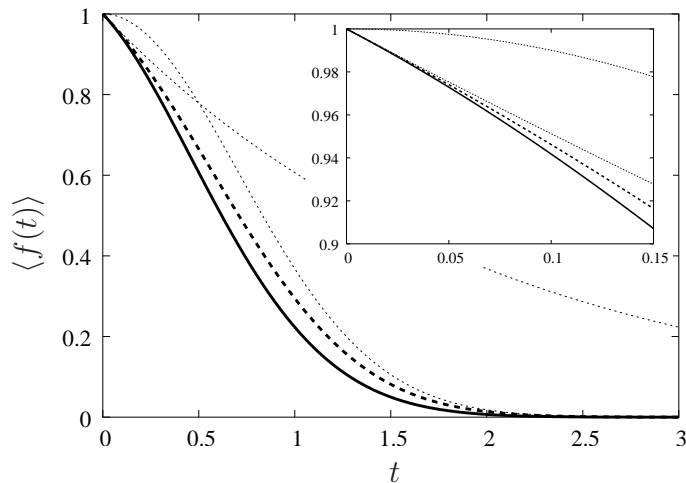


Figure 2. The fidelity amplitude in the crossover regime, from linear to quadratic decay. $2\pi\lambda = 1$. Thick solid and dashed lines: Theory for the Poisson and the GOE case respectively, *i.e.* equation (15) packed into an exponential (see text for details). Thin dotted lines: Theory for the Poisson case, where either the linear term or the quadratic term has been ignored. The inset shows a zoom into the area around $t = 0$, $\langle f(t) \rangle = 1$.

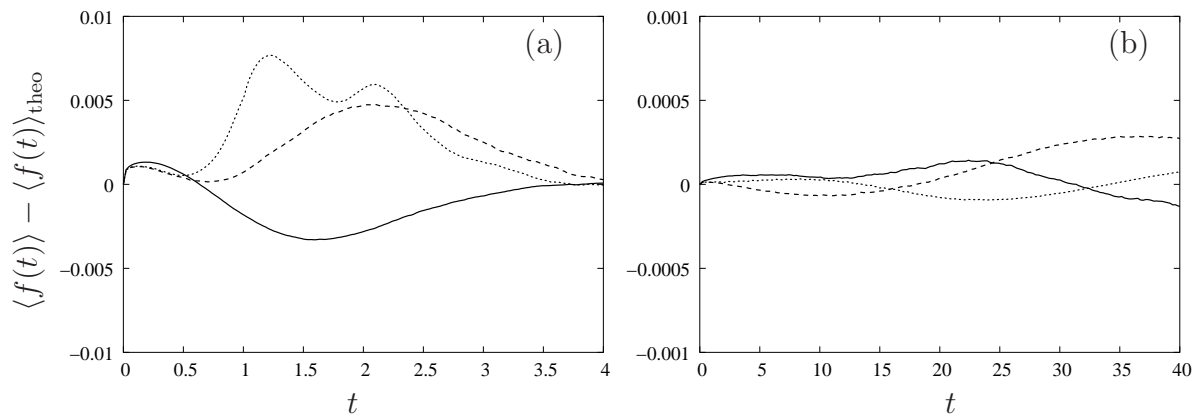


Figure 3. Difference between the Monte Carlo and the theoretical result, equation (18), for the fidelity amplitude, for the Poisson (solid line), the GOE (dashed line) and the picket-fence (dotted line) case. In (a) $\lambda = 0.1$, whereas in (b) $\lambda = 0.01$ (note the different scale on the ordinate).

above the Poisson ones due to the correlations in the spectrum of H_0 . The crossover region is precisely the one of most interest and, therefore, we check the accuracy of the phenomenological expression (18) beyond the perturbative limit.

Figure 3 shows the deviation of the fidelity amplitude obtained for Monte Carlo calculations for $N = 100$ from what we find using equation (18) and the $N = \infty$ correlation integral. Besides the GOE case, we considered also spectra without correlations (Poisson case) and a spectrum with equally spaced levels (picket-fence case).

In this way we cover a broad range of possible spectral correlations. For $\lambda = 0.1$, figure 3(a), the deviations are of the order 0.5% of the maximal value for the fidelity amplitude. We checked that these deviations are not due to finite size effects. By varying N and also by considering the correlation integrals for finite N (for the Poisson and the picket-fence case), we found that those effects do not alter the error noticeably, except for a small “hump” at $t \approx 0.25$ in panel (a). In panel (b), the error is shown for $\lambda = 0.01$. Its absolute value is further reduced by a factor of ten, roughly, and finite size effects are no longer observable. Note that the errors for the random and the picket-fence spectrum are of the same order of magnitude as for the chaotic case. This suggests, that our exponentiated formula works well in all cases, where the two-point correlations are known. In order to compare the error curves in figure 3 with the actual value of the fidelity amplitude, note that the time t_{half} where the fidelity has dropped to half of its initial value is about $t_{\text{half}} \approx 1.1$ in panel (a), and $t_{\text{half}} \approx 13$ in panel (b). In all, we see that the results shown in figure 2 are very similar to what we can expect from a Monte Carlo calculation.

2.4. Sample fluctuations

In the figures 1 and 2 we saw the effects of spectral correlations on the decay of the average fidelity. But are these effects observable also for an individual system? To answer this question, we shall now study the fluctuations of the fidelity amplitude, focusing on the regime of high fidelity.

To obtain the numerical results shown in figure 3 and hereafter, we average over the GOE perturbation V , the spectrum of H_0 and eventually over initial states \hat{x} . The initial state may be an eigenstate of H_0 ; then we choose it from the centre of the spectrum in order to minimise border effects. Alternatively, it may be a random (orthogonally invariant) state. Though the average value of the fidelity amplitude does not depend on the choice of the initial state, higher moments (such as the variance) do.

Figure 4 shows the average fidelity amplitude $\langle f(t) \rangle$ in the perturbative regime for the Poisson and the GOE case. We performed 10 independent ensemble averages, each of them over $n_{\text{run}} = 1000$ random systems. From this we calculated the statistical uncertainty for a single ensemble average. In this figure, as well as in similar ones below, the area which is not more than one (two) standard deviations away from the total average over all samples, is plotted in dark (light) gray. In addition, we plotted the pure linear response result, equation (15) for the Poisson ensemble (solid line) and the GOE (dashed line). While in panel (a), we show $f(t)$ itself, in panel (b), the Poisson theory is subtracted in order to show more clearly the differences between the Poisson and the GOE case on the one hand, as well as between numerics and linear response theory on the other.

The large sample-to-sample fluctuations are clearly due to the special choice of the initial state. In linear response theory, and after the averaging over V , it can be seen that the fidelity amplitude depends on only N out of $N(N - 1)$ available eigenvalue

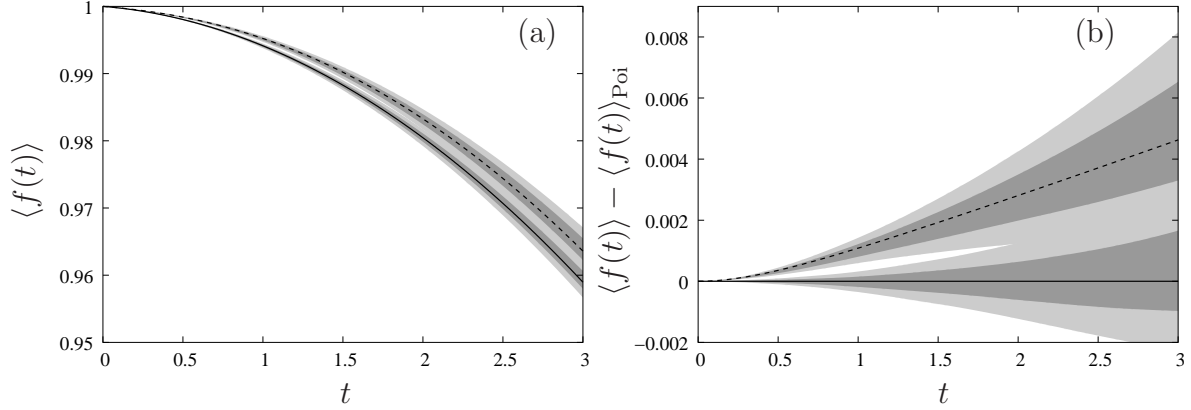


Figure 4. (a) Fidelity amplitude for $N = 100, \lambda = 0.01$; the initial states are eigenstates of H_0 . The thick solid and dashed lines show the theoretical result (15) for the Poisson and the GOE case, respectively. The numerical results (shaded areas) are obtained from 10 small sample averages of size $n_{\text{run}} = 1000$, each. The total average of all samples lies in the centre of the gray bands, while their borders are given by plus/minus one standard deviation (dark gray), and plus/minus two standard deviations (light gray). (b) The same quantities as in (a), but with the Poisson theory subtracted.

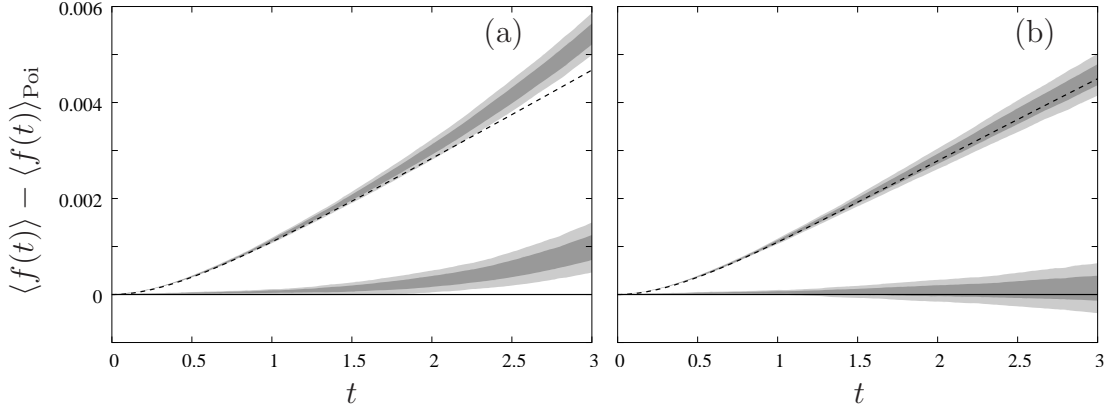


Figure 5. Fidelity amplitude with the Poisson theory subtracted, for $N = 100, \lambda = 0.01$; random initial states. The numerical results (shaded areas) are obtained from 10 small samples of size $n_{\text{run}} = 1000$, each. The significance of the gray scales is the same as in figure 4. (a) The thick solid and dashed lines show the theoretical results for the Poisson case (here, we expect zero) and the GOE case, based on the linear response result (15). (b) The same data, but with the linear response result being packed into an exponential (18).

differences [see equation (10)]. By consequence, we need very large samples in order to obtain accurate averages. However, the statistical fluctuations can also be reduced by probing the decay of $f(t)$ at the same system for various initial H_0 -eigenstates, or by using a random initial state, as shown below.

Figure 5 shows the fidelity amplitude (with the Poisson theory subtracted), for the

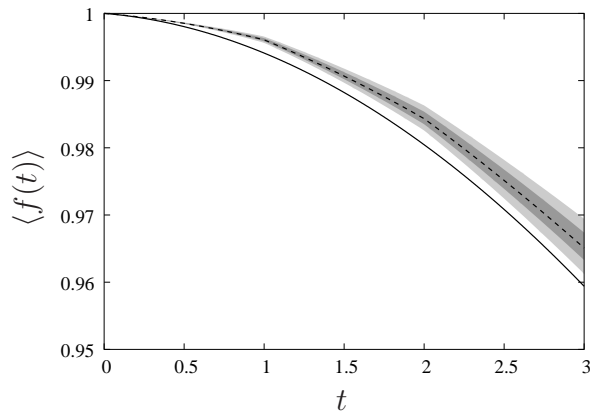


Figure 6. Fidelity amplitude for $N = 100, \lambda = 0.01$; small samples of size $n_{\text{run}} = 1000$. The numerical results are represented by shaded bands, where the significance of the gray scales is the same as in figure 4. Data for the picket-fence spectra, where the initial states are eigenstates of H_0 . The linear response result (15) for the Poisson case (thick solid line) and the picket-fence case (thick dashed line).

Poisson and the GOE case, where the initial states are taken to be random. We used the same sample size as in figure 4. Nevertheless, the statistical fluctuations have drastically decreased, and the Poisson- and the GOE-data can now be distinguished without difficulty. While in panel (a) we used the pure linear response theory, equation (15), for the Poisson and the GOE case, in panel (b), we used the exponentiated version, equation (18). One can clearly see that there are systematic differences between the numerical data and pure linear response theory, while we obtained a near perfect agreement with the help of the exponentiation.

Using a result from the following section 3, one can understand the reduction of the statistical fluctuations. According to equation (28), the variance of the fidelity amplitude is proportional to the IPR of the initial state. As for a random state $\hat{x} : \text{ipr}(\hat{x}) = 3/(N + 2)$, it implies that the statistical deviations should be about $\sqrt{(N + 2)/3} \approx 6$ times smaller than in figure 4(b). We finally note that the error which remains after exponentiating equation (15) is so small, that it will typically be lost in these fluctuations.

From figure 6 we can see that, also for the picket-fence spectra, the linear response theory does a good job. What is more interesting, is a comparison of the statistical deviations of the numerical curves for this figure, and figure 4(a) which is practically the same plot, but for the Poisson and the GOE spectra. As the spectrum in the picket-fence case is no statistical quantity, it means that the statistical deviations are mainly due to the fluctuations in the perturbation matrix V . This implies that the fidelity decay is sensitive to the level correlations in a single spectrum (of very moderate length, $N = 100$). One would just have to probe this particular system with different initial states, and different perturbations. Quantum dots with variable magnetic fields may be an appropriate test ground.

From the numerical analysis of the sample fluctuations, as well as from the linear response result for the variance of the fidelity amplitude, we conclude that the sample fluctuations are proportional to the inverse participation ratio of the initial state \hat{x} . To observe a significant difference between a GOE spectrum and a spectrum without correlations, we need either very large samples (for initial H_0 -eigenstates), or initial states with very small inverse participation ratio (*e.g.* random initial states). The sample fluctuations are mainly due to the randomness of the perturbation V , not so much due to the random H_0 . Finally, we have verified that the exponentiation of the linear response result improves the agreement with numerics considerably. In section 2.5 to follow, we will perform a further, more realistic, test.

2.5. A deterministic example

In reference [13] Cerruti and Tomsovic calculate the fidelity amplitude for the quantised standard map. They also present an analytical formula for the decay of the fidelity amplitude, which is based on a “uniform approximation”. In essence, they use a random matrix model similar to ours, and an additional semiclassical argument which allows them to determine the perturbation strength. Their final formula agrees with ours in both limit cases of weak and strong perturbation, if we disregard the spectral correlations, *i.e.* if we set the two-point form factor in the correlation integral, equation (14), equal to zero. However, in the crossover region, there are further deviations.

In order to compare our approach to theirs, we first have to adapt our model to a two-fold symmetry in the standard map, which leads to two independent symmetry sectors in the Hamiltonian. This influences the correlation integral, and by re-examining equation (10), we obtain:

$$\mathcal{C}_{\text{sym}}(t) = t^2 + \frac{1}{4} \left[t - \int_0^t d\tau \int_0^\tau d\tau' b_2^{\text{GOE}}(\tau') \right], \quad (19)$$

where the unit for time is again chosen such that $t_H = 1$. Finally, we have to take into account that our strength parameter λ , is related to Cerruti and Tomsovic’s by: $\lambda^2 = 4\Lambda$, and that in reference [13] the unit for time is chosen differently. In all, we obtain for the fidelity amplitude:

$$f_{\text{sym}}(t) = \exp[-16\pi^2\Lambda\mathcal{C}_{\text{sym}}(t)], \quad (20)$$

where Cerruti and Tomsovic’s semiclassical argument gives $\Lambda \approx 0.0395$. The same result follows also from general considerations of [4].

In figure 7 we reproduce the numerical data for the quantised standard map from Cerruti and Tomsovic, and compare it with a random matrix calculation and our theory, equation (20). In the random matrix model we choose a matrix of dimension $N = 1000$, which is block-diagonal. Each block contains a matrix of dimension $N/2$, produced from an unfolded GOE spectrum (with average level spacing equal to two) and a GOE perturbation, as defined earlier. The variance of the non-zero off-diagonal matrix

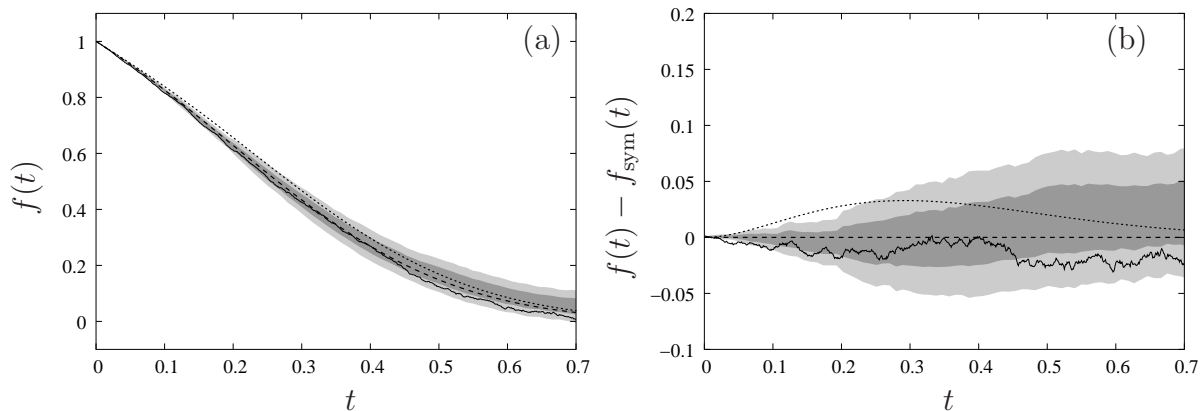


Figure 7. (a) The fidelity amplitude for the quantised standard map (data from [13]) (solid line). Our exponentiated linear response result, equation (20) for $\Lambda = 0.0395$ (dashed line), and the theoretical result of Cerruti and Tomsovic (dotted line). The average over the full sample lies in the centre of the gray bands, while their borders are given by plus/minus one standard deviation (dark gray), and plus/minus two standard deviations (light gray). (b) The same curves as in (a) but with our theory, equation (20), subtracted.

elements is $\lambda^2 = 4\Lambda$. To estimate the statistical error on the fidelity amplitude, we calculated $f(t)$ for ten different random matrices of this type. In addition, we plot the corrected theoretical result from Cerruti and Tomsovic [13].

The fidelity decay for the quantised standard map is well described by our random matrix model. In particular in panel (b) we can see that the corresponding curve stays well within the statistical limits for individual members of the random matrix ensemble. Though our theory is not exact (cf. figure 3, and note that $\lambda \approx 0.4$ is quite large), the systematic deviations from the random matrix results, as well as from the quantised standard map calculation, are very small. The theory of Cerruti and Tomsovic shows somewhat larger systematic deviations, in particular in the region around $t = 0.2$. Note that we compare with the semiclassical result of reference [13], because we use the same classical parameters in our random matrix model.

3. The fidelity

In an experiment it is usually easier to measure the fidelity $F(t) = |f(t)|^2$ rather than the fidelity amplitude. Though, often it is assumed that the average fidelity is simply given by the absolute value squared of the average fidelity amplitude, and we shall see under which conditions this is justified. In distinction to the average amplitude, the average fidelity depends on the choice of the initial state. For instance, if the initial state is an eigenstate of H_0 , the fidelity $F(t)$ coincides with the survival probability or autocorrelation function.

3.1. Linear response

In order to calculate the fidelity $F(t)$, we first expand the linear response approximation of the echo operator (8) according to increasing powers of λ :

$$X(t) = 1 - 2\pi i \lambda I(t) - 4\pi^2 \lambda^2 J(t) , \quad (21)$$

$$I(t) = \int_0^t d\tau \tilde{V}(\tau) \quad J(t) = \int_0^t d\tau \int_0^\tau d\tau' \tilde{V}(\tau) \tilde{V}(\tau') . \quad (22)$$

For an arbitrary initial state $\overset{\circ}{x}$, the average fidelity reads:

$$\langle F(t) \rangle_V = \langle \langle X(t) \rangle_{\overset{\circ}{x}} \langle X(t) \rangle_{\overset{\circ}{x}}^* \rangle_V = 1 - 4\pi^2 \lambda^2 (2\text{Re} \langle \langle J(t) \rangle_{\overset{\circ}{x}} \rangle_V - \langle |\langle I(t) \rangle_{\overset{\circ}{x}}|^2 \rangle_V) , \quad (23)$$

where we considered only terms up to second order. For the average $\langle \langle J(t) \rangle_{\overset{\circ}{x}} \rangle_V$ we obtain (cf. section 2.1):

$$\langle J_{\alpha\beta}(t) \rangle_V = \delta_{\alpha\beta} \int_0^t d\tau \int_0^\tau d\tau' C_\alpha(\tau - \tau') = \delta_{\alpha\beta} \int_0^t d\tau \int_0^\tau d\tau' C_\alpha(\tau') , \quad (24)$$

while

$$\langle |\langle I(t) \rangle_{\overset{\circ}{x}}|^2 \rangle_V = \sum_{\alpha\beta\gamma\varepsilon} \overset{\circ}{x}_\alpha^* \overset{\circ}{x}_\beta \overset{\circ}{x}_\gamma \overset{\circ}{x}_\varepsilon^* \int_0^t d\tau \int_0^\tau d\tau' \langle \tilde{V}_{\alpha\beta}(\tau) \tilde{V}_{\gamma\varepsilon}^*(\tau') \rangle_V . \quad (25)$$

The average product of two matrix elements of \tilde{V} can be computed with the help of equation (9). For the GOE perturbation, we obtain:

$$\begin{aligned} \langle \tilde{V}_{\alpha\beta}(\tau) \tilde{V}_{\gamma\varepsilon}^*(\tau') \rangle_V &= [\delta_{\alpha\gamma} \delta_{\beta\varepsilon} \Delta_\alpha(-\tau + \tau') \Delta_\beta(\tau - \tau') + \delta_{\alpha\varepsilon} \delta_{\beta\gamma} \Delta_\alpha(-\tau - \tau') \Delta_\beta(\tau + \tau')] \\ &= \left[\delta_{\alpha\gamma} \delta_{\beta\varepsilon} e^{2\pi i(\overset{\circ}{E}_\alpha - \overset{\circ}{E}_\beta)(\tau - \tau')} + \delta_{\alpha\varepsilon} \delta_{\beta\gamma} e^{2\pi i(\overset{\circ}{E}_\alpha - \overset{\circ}{E}_\beta)(\tau + \tau')} \right] \\ &= \begin{cases} 2 & : \alpha = \beta = \gamma = \varepsilon \\ e^{2\pi i(\overset{\circ}{E}_\alpha - \overset{\circ}{E}_\beta)(\tau - \tau')} & : \alpha = \gamma \neq \beta = \varepsilon \\ e^{2\pi i(\overset{\circ}{E}_\alpha - \overset{\circ}{E}_\beta)(\tau + \tau')} & : \alpha = \varepsilon \neq \beta = \gamma \\ 0 & : \text{otherwise} \end{cases} , \end{aligned} \quad (26)$$

which leads to

$$\begin{aligned} \langle |\langle I(t) \rangle_{\overset{\circ}{x}}|^2 \rangle_V &= \int_0^t d\tau \int_0^\tau d\tau' \left[2 \sum_\alpha |\overset{\circ}{x}_\alpha|^4 \right. \\ &\quad \left. + \sum_{\alpha \neq \beta} \left(|\overset{\circ}{x}_\alpha|^2 |\overset{\circ}{x}_\beta|^2 e^{2\pi i(\overset{\circ}{E}_\alpha - \overset{\circ}{E}_\beta)(\tau - \tau')} + (\overset{\circ}{x}_\alpha^*)^2 \overset{\circ}{x}_\beta^2 e^{2\pi i(\overset{\circ}{E}_\alpha - \overset{\circ}{E}_\beta)(\tau + \tau')} \right) \right] . \end{aligned} \quad (27)$$

Here $\sum_\alpha |\overset{\circ}{x}_\alpha|^4 = \text{ipr}(\overset{\circ}{x})$ is the inverse participation ratio (IPR) of the initial state $\overset{\circ}{x}$. If the initial state is an eigenstate of H_0 , then $\text{ipr}(\overset{\circ}{x}) = 1$, and this is the only term which survives. If $\overset{\circ}{x}$ is complex, then we expect that term which depends on $(\tau + \tau')$ to vanish. On the average, the contribution of each of the exponential terms is only of order N^{-1} .

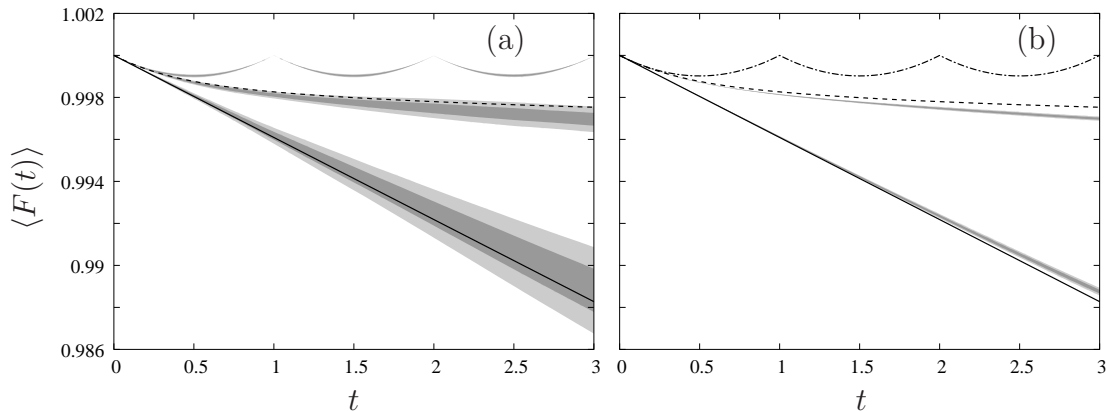


Figure 8. Fidelity for $N = 100, \lambda = 0.01$; the initial states are eigenstates of H_0 . (a) The thick solid and dashed lines show the linear response result (28) for the Poisson case and the GOE case, respectively. The numerical results (shaded areas) are obtained from 10 small samples of size $n_{\text{run}} = 1000$, each. The picket-fence case is also included. The total average of all samples lies in the centre of the gray bands, while their borders are given by plus/minus one standard deviation (dark gray), and plus/minus two standard deviations (light gray). (b) As in (a) but for 10 large samples of size $n_{\text{run}} = 50\,000$. In the picket-fence case, the theoretical result is plotted (thick dash-dotted line) instead of the numerical data.

Therefore, the whole expression in the second line of equation (27) is of order N^{-1} . In the limit of large N , it can be neglected, leading to

$$\begin{aligned} \langle F(t) \rangle_V &= 1 - 2(2\pi\lambda)^2 \left\{ \mathcal{C}(t) - \text{ipr}(\overset{\circ}{x}) t^2 \right\} \\ &= |\langle f(t) \rangle_V|^2 + 2(2\pi\lambda)^2 t^2 \text{ipr}(\overset{\circ}{x}) + \mathcal{O}(t^4). \end{aligned} \quad (28)$$

For the GUE perturbation, equation (26) would simply read: $\langle \tilde{V}_{\alpha\beta}(\tau) \tilde{V}_{\gamma\epsilon}^*(\tau') \rangle_V = \delta_{\alpha\beta} \exp[2\pi i(\overset{\circ}{E}_\alpha - \overset{\circ}{E}_\beta)(\tau - \tau')]$. For the average fidelity, it would have the only consequence that all terms involving $\text{ipr}(\overset{\circ}{x})$ had to be multiplied by one half.

The second line of equation (28) gives the variance of the sample fluctuations of the fidelity amplitude, discussed in the previous section. It shows that, if the IPR of the initial state goes to zero, then indeed, the average fidelity is given by the absolute value squared of the fidelity amplitude (at least in the linear response regime). By contrast, if the IPR of the initial state is large (few principal components), then the behaviour of the fidelity is quite different from that of the fidelity amplitude. In the extreme case that the IPR is equal to one (initial state is an eigenstate of H_0), the IPR-term in equation (28) completely kills the t^2 -term in the correlation integral $\mathcal{C}(t)$. This holds equally true whether V is chosen from the GOE or the GUE.

3.2. Average fidelity and sample-to-sample fluctuations

In figure 8 we show the fidelity decay for states which are initially eigenstates of H_0 . Due to the cancellation of the t^2 -terms, the fidelity decays much slower, and the effects of the

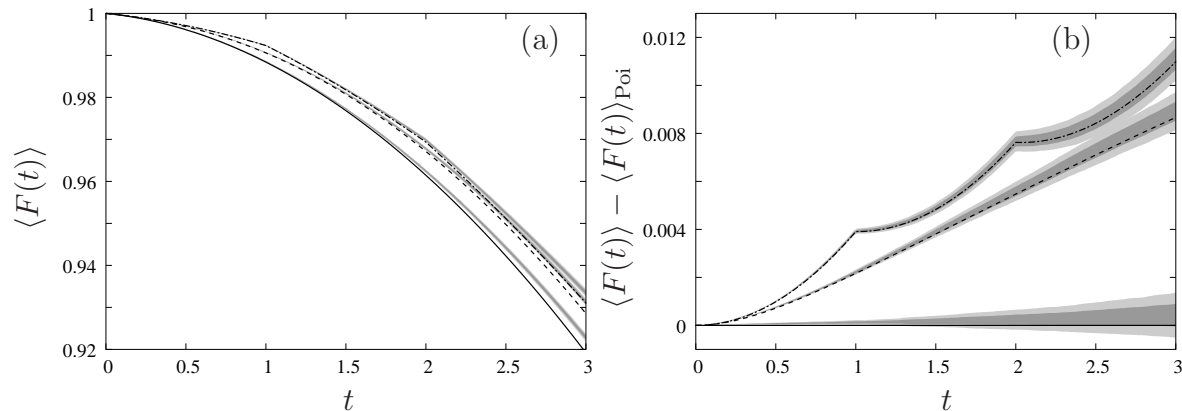


Figure 9. Fidelity for $N = 100, \lambda = 0.01$; random initial states. Results for 10 small samples of size $n_{\text{run}} = 1000$. The numerical results are represented by shaded bands, where the significance of the gray scales is the same as in figure 8. (a) Data for the Poisson case, the GOE-case, and the picket-fence case. The thick lines give the theoretical results for the Poisson case (thick solid line), the GOE-case (thick dashed line), and the picket-fence case (dash-dotted line). (b) As in (a) but with the Poisson theory subtracted (linear response, packed into an exponential).

spectral correlations are more pronounced. For example, for the picket-fence spectrum, we get practically complete revivals at integer multiples of the Heisenberg time, while in the Poisson case, the fidelity decays linearly. Note that exact revivals can occur in the perturbative limit, only. There the eigenvectors of H are arbitrarily well approximated by the eigenvectors of H_0 . The statistical deviations seem to be much smaller in the picket-fence case; see figure 8(a). However, this is simply because the fidelity is closer to one. We checked that the relative error for the correlation integral, remains comparable for all three cases.

In figure 8(b) one can see a small difference between the theoretical linear response result and the numerics for both, the Poisson and the GOE case. This time, it does not help to exponentiate the linear response result. Here, the fidelity decay is too slow to produce an observable effect. Note also that the deviations differ in sign. While the theory underestimates the fidelity decay in the GOE case, it overestimates the decay in the Poisson case. This points at a more complicated behaviour of the fidelity (as compared to the fidelity amplitude). In the picket-fence case, by contrast, the difference between theory and numerical result is much too small to be resolved. Due to the fact that the statistical fluctuations have also diminished, we decided not to show the numerics at all.

In figure 9 we show the behaviour of the fidelity for random initial states. As expected, the fidelity behaves very similar to the fidelity amplitude in this case (*cf.* figures 4 and 5). Its decay is again dominated by the t^2 -term, and the effect of the correlations in the spectrum of H_0 has decreased, as compared to figure 8. Again, it makes sense to exponentiate the linear response result, in analogy to equation (18).

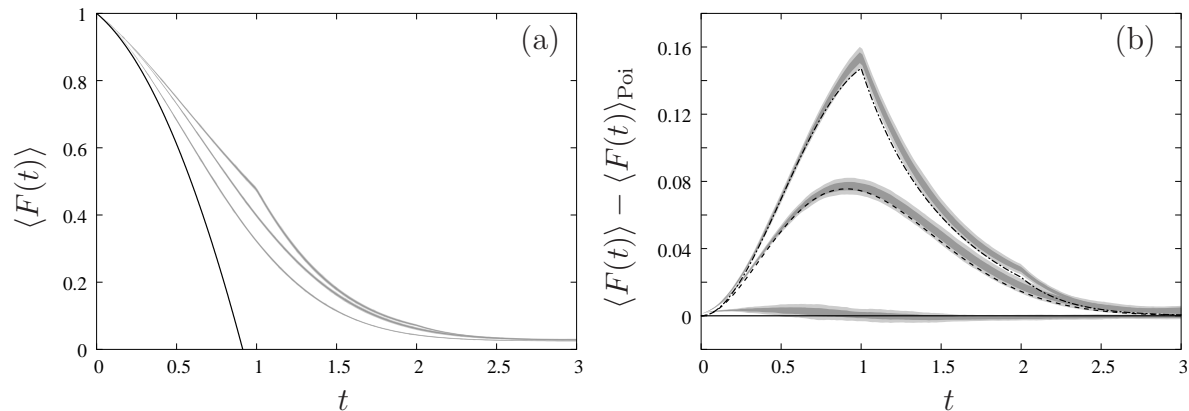


Figure 10. Fidelity for $N = 100, \lambda = 0.1$; random initial states. Results for 10 small samples of size $n_{\text{run}} = 1000$. The numerical results are represented by shaded bands, as in figure 8. (a) Numerical results for the Poisson case, the GOE-case, and the picket-fence case. The thick solid line shows the pure linear response result for the Poisson case. (b) as in (a), but with the Poisson theory subtracted (linear response, packed into an exponential). The theoretical results, using equation (29), are shown for the Poisson case (thick solid line), GOE-case (thick dashed line), and the picket-fence case (thick dash-dotted line).

Figure 10 shows the fidelity decay for random initial states in the crossover regime, $\lambda = 0.1$, between perturbative and golden rule decay. According to the discussion of the figures 1 and 2, we expect a stronger effect of the spectral correlations in this regime. Note *e.g.* at the Heisenberg time, $t = 1$, the relative differences between Poisson and GOE as well as between GOE and picket-fence, are of the order of 10%, each. The theoretical curve in figure 10(a) is the pure linear response result. It is obviously not sufficiently accurate. To improve, we use exponentiation, but in addition we also take into account a rather trivial finite size effect: Namely, as will be shown in the following section: $\lim_{t \rightarrow \infty} F(t) = c_{\infty} \approx 3/(N+2)$. Therefore, instead of the simple exponentiation, we use

$$h(x) = (1 - c_{\infty}) e^{-x/(1-c_{\infty})} + c_{\infty}, \quad c_{\infty} \approx \frac{3}{N+2}. \quad (29)$$

This phenomenological formula describes the numerical results quite well, as can be seen in figure 10(b).

In all the cases considered, we find that the spectral correlations (or more precisely, the level repulsion) tend to attenuate fidelity decay. Qualitatively, this can be understood from standard perturbation theory [18], which relates changes in the eigenvector components of H to the matrix elements of the perturbation $\lambda V_{\alpha\beta}$, weighted with the inverse level distance $(\overset{\circ}{E}_{\alpha} - \overset{\circ}{E}_{\beta})^{-1}$. Accordingly, the fidelity decay is slowest in the picket-fence case. In the GOE case (which may be associated with chaotic dynamics) it is somewhat faster, while in the Poisson case (characteristic of integrable dynamics) it is

fastest. In this sense, we can confirm that fidelity is more likely to be maintained, if the system's dynamics is chaotic rather than integrable. This, at first sight counter-intuitive result, has been obtained previously by a number of authors [4, 14, 17], although along quite different lines of argument.

3.3. Fidelity distributions

In particular for eigenstates of H_0 , we saw a dramatic effect of the spectral correlations on the decay of the average fidelity. As it turned out, sufficiently strong correlations can practically stop the decay of $\langle F(t) \rangle$ at values quite close to one (cf. figure 8). However, the large sample-to-sample fluctuations in this case make us suspect that for individual systems this stabilisation effect might be reduced, or not even observable. However, in the case of the fidelity amplitude, we could actually prove that if the IPR of the initial state is only small enough, then effects of the spectral correlations are observable even for individual systems. We expect that the situation will be similar in the case of the fidelity itself. There will be a trade off between quantum ergodicity and the size of spectral correlations. Besides of its own interest, we study the fidelity distributions $P(F(t))$ to clarify this point. We generate the required histograms at certain equidistant time instances. For each histogram, the interval $(0, 1]$ is divided into 50 boxes. Then, for a certain sample of n_{run} systems we count the frequencies with which the fidelity for an individual system, at a given time, falls into one of those boxes. After proper normalisation the histograms are lined up along the time axis, which results in three dimensional plots.

In figure 11 we focus on the qualitative features of the fidelity distribution for different choices of the initial states. For simplicity we show the Poisson case, though note that our observations are equally valid for the GOE case. In all three panels we show the fidelity distribution as it evolves in time, together with the behaviour of the average fidelity (thick dashed line in the xy -plane). For H_0 -eigenstates, panel (a), the maximum of the distribution remains very close to one, while its average continues to decay (very slowly, though). In this case, linear response predicts a purely linear decay, which can be observed at small times. However, for larger times $t \gtrsim 0.3$ the average fidelity starts to saturate, an effect we cannot describe theoretically (as we noticed already in figure 8, exponentiation does not help, here). The separation between the average and the maximum of the fidelity distribution is due to the development of a long range tail.

For random initial states, panel (b), the fidelity distribution is rather symmetric around its average value. Its shape looks almost Gaussian. We checked that the width of the distribution decreases roughly proportional to $1/\sqrt{N}$. This means that we have true quantum ergodicity for the fidelity of a random initial state. For sufficiently high dimension of the Hamiltonian, the sample-to-sample fluctuations can be made arbitrarily small.

In panel (c), we show the fidelity distribution, where, for each individual system,

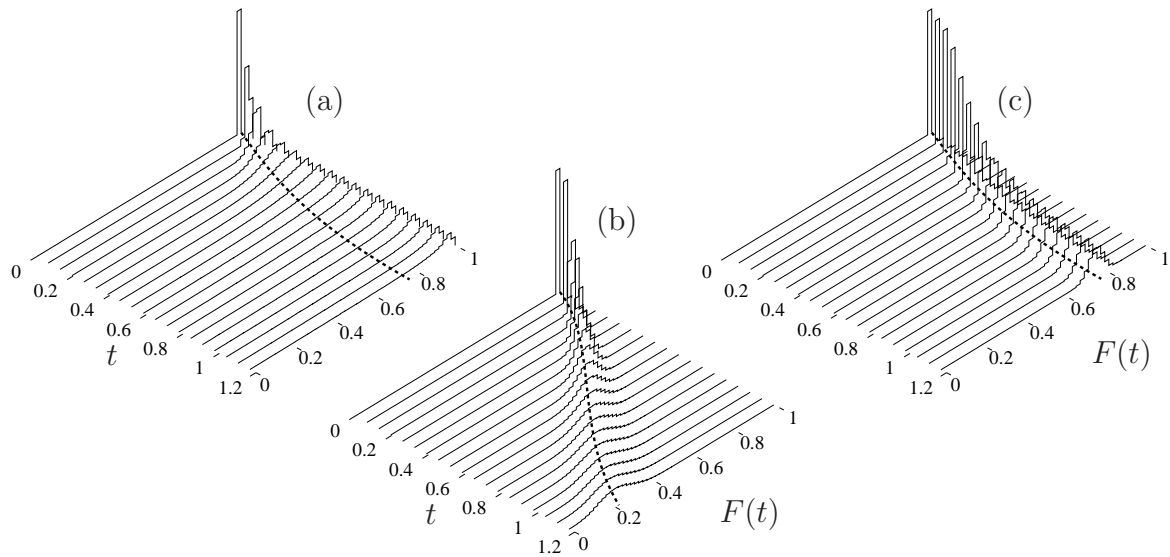


Figure 11. Fidelity distribution for $N = 100$, $\lambda = 0.1$ for the Poisson case. Histogram as a function of time (solid lines), for initial eigenstates (a), for random initial states (b), and for the average over all possible initial eigenstates (c). The distributions are normalised, such that *e.g.* at $t = 0$ the height of the bar is 50, because the widths of the histogram boxes is $1/50$. The average fidelity is plotted as a thick dashed line in the xy -plane.

we have averaged over all available H_0 -eigenstates as initial states. This also reduces the sample-to-sample fluctuations drastically. Though, qualitatively, the width of the fidelity distribution behaves similar to the case with random initial states, it is noticeably smaller. Of course, the average fidelity shows here exactly the same behaviour as in panel (a).

In figure 12 we show examples of fidelity distributions for the Poisson, the GOE, and the picket-fence case, at three different times t_1 , t_2 , and t_3 . At a time $t_1 = 0.195$ much before the Heisenberg time, at Heisenberg time $t_2 = 0.974$ and at a time much after the Heisenberg time $t_3 = 1.884$. The different panels are arranged into columns, where in the left column we used H_0 -eigenstates as initial states, in the middle column we used random initial states, and in the right column, we averaged over all H_0 -eigenstates.

In the left column we clearly see the development of a long range tail towards low fidelities, which causes the separation between the average and the maximum of the fidelity distribution. Though the tail is more pronounced in the Poisson case, it is still important in the GOE case, but may be somewhat less important in the picket-fence case. In the middle and the right column, the fidelity distributions have almost perfect symmetric shapes, at least as long as the distributions do not come too close to the boundaries zero and one. In the case where we averaged over the H_0 -eigenstates (right column), the widths of the distributions are small enough to allow to distinguish even

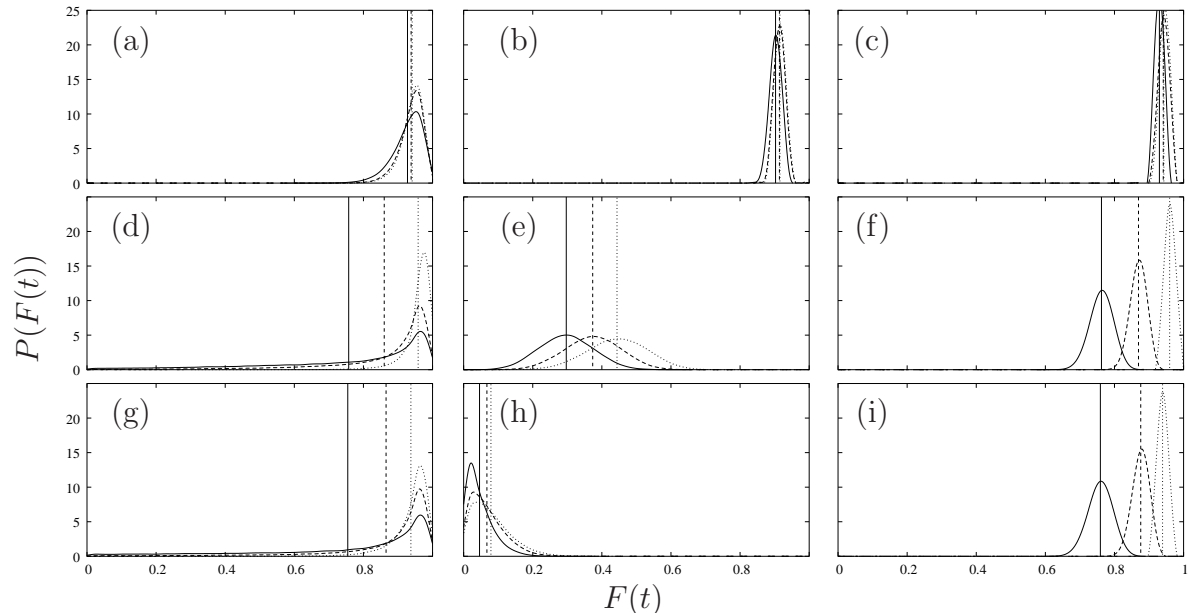


Figure 12. Fidelity distributions for $N = 100$, $\lambda = 0.1$ for the Poisson case (solid line), the GOE case (dashed line), and the picket-fence case (dotted line) at three different times: $t = 0.195$ [(a),(b),(c)], $t = 0.974$ [(d),(e),(f)], and $t = 1.884$ [(g),(h),(i)]. In the left column [(a),(d),(g)], the initial states were eigenstates of H_0 , in the middle column [(b), (e), (h)] we used random initial states, and in the right column [(c),(f),(i)] we averaged over all initial eigenstates of H_0 . The vertical lines give the average value of the fidelity for the whole sample for the Poisson case (solid line), for the GOE case (dotted line), and for the picket-fence case (dashed line).

individual systems with respect to the different spectral correlations. For random initial states (middle column), the widths of the fidelity distributions are not small enough, and one would have to use bigger Hamiltonian matrices ($N \gtrsim 1000$).

4. The fidelity in the long time limit

Here we will calculate the survival probability, the fidelity amplitude, and the fidelity in the limit $t \rightarrow \infty$ (with the strength of the perturbation held fixed). One may think that in general, only the eigenvectors are important. As will be shown below, this is indeed the case, as long as H_0 is not constructed from a picket-fence spectrum. We use time independent perturbation theory, to obtain approximations to the eigenvectors. The details can be found in Appendix B.

Remember that we are using units for time and energy such that the Heisenberg time and the mean level spacing are both equal to one (see section 2). In these units, the time dependent Schrödinger equation reads:

$$i\partial_t \Psi(t) = 2\pi (H_0 + \lambda V) \Psi(t) = 0. \quad (30)$$

Suppose we can diagonalise $H = H_0 + \lambda V$ exactly. Then, an initial state $\overset{\circ}{x}$ will evolve

in time according to

$$u(t) = O \Delta(t) O^T \overset{\circ}{x}, \quad \Delta(t) = \text{diag}(e^{-2\pi i E_\alpha t}), \quad O^T H O = \text{diag}(E_\alpha). \quad (31)$$

We assume that H_0 is diagonal, so that we obtain for the evolution in the interaction picture:

$$x(t) = \Delta_0(t)^{-1} u(t) = \Delta_0(-t) O \Delta(t) O^T \overset{\circ}{x}, \quad \Delta_0(t) = \text{diag}(e^{-2\pi i \overset{\circ}{E}_\alpha t}), \quad (32)$$

where $\overset{\circ}{E}_\alpha$ are the eigenvalues of H_0 . Here, $\Delta_0(-t) O \Delta(t) O^T$ is the exact echo operator introduced in equation (1). We expect, that in the long time limit, all dependencies on the eigenvalues of H and H_0 will drop out, so that the problem consists in finding an appropriate approximation for the eigenvectors, *i.e.* for the orthogonal matrix O .

The fidelity amplitude can be expressed as the expectation value of the echo operator with respect to the state $\overset{\circ}{x}$.

$$f(t) = \langle \Delta_0(-t) O \Delta(t) O^T \rangle_{\overset{\circ}{x}} = \sum_{\alpha\beta\gamma} \overset{\circ}{x}_\alpha e^{2\pi i \overset{\circ}{E}_\alpha t} O_{\alpha\beta} e^{-2\pi i E_\beta t} O_{\gamma\beta} \overset{\circ}{x}_\gamma. \quad (33)$$

In this expression, the phases in the exponential can never cancel. Therefore, the fidelity amplitude, averaged over the perturbation V and over H_0 , vanishes in the limit $t \rightarrow \infty$.

$$\lim_{t \rightarrow \infty} \langle f(t) \rangle_{0,V} = 0. \quad (34)$$

For the fidelity, we obtain a more complicated expression:

$$\begin{aligned} F(t) &= \left| \sum_{\alpha\beta\gamma} \overset{\circ}{x}_\alpha e^{2\pi i \overset{\circ}{E}_\alpha t} O_{\alpha\beta} e^{-2\pi i E_\beta t} O_{\gamma\beta} \overset{\circ}{x}_\gamma \right|^2 \\ &\rightarrow \sum_{\alpha\alpha'} \sum_{\beta} \sum_{\gamma\gamma'} \overset{\circ}{x}_\alpha \overset{\circ}{x}_{\alpha'} e^{2\pi i (\overset{\circ}{E}_\alpha - \overset{\circ}{E}_{\alpha'}) t} O_{\alpha\beta} O_{\alpha'\beta} O_{\gamma\beta} O_{\gamma'\beta} \overset{\circ}{x}_\gamma \overset{\circ}{x}_{\gamma'}. \end{aligned} \quad (35)$$

Here, the arrow indicates that we discarded already those terms containing phases of the form $\exp[-2\pi i (E_\beta - E_{\beta'}) t]$, as they cannot contribute to the long time limit of the average fidelity.

If $\overset{\circ}{x}$ is an eigenstate of H_0 , $\overset{\circ}{x}_\beta = \delta_{\alpha\beta}$, then the fidelity as a function of time coincides with the survival probability, as we have seen in the beginning of section 3. For the limit value of both quantities, we thus get:

$$F_\infty^e = \lim_{t \rightarrow \infty} \langle F(t) \rangle_{0,V} = \lim_{t \rightarrow \infty} \langle S(t) \rangle_{0,V} = \sum_{\xi} \langle O_{\alpha\xi}^4 \rangle_{0,V} = \langle \text{ipr}(O^T \overset{\circ}{x}) \rangle_{0,V}. \quad (36)$$

This is the inverse participation ratio of the local density of states (*i.e.* the projections of the H_0 -basis state onto the eigenbasis of H). By contrast, if $\overset{\circ}{x}$ is a random state, $\langle F(t) \rangle_{0,V} \rightarrow F_\infty^r$, where:

$$F_\infty^r = \sum_{\alpha \neq \gamma} \sum_{\beta} \left\langle \overset{\circ}{x}_\alpha^2 O_{\alpha\beta}^2 O_{\gamma\beta}^2 \overset{\circ}{x}_\gamma^2 \right\rangle_{0,V} + \sum_{\alpha \neq \alpha'} \sum_{\beta} \left\langle \overset{\circ}{x}_\alpha^2 \overset{\circ}{x}_{\alpha'}^2 e^{2\pi i (\overset{\circ}{E}_\alpha - \overset{\circ}{E}_{\alpha'}) t} O_{\alpha\beta}^2 O_{\alpha'\beta}^2 \right\rangle_{0,V}$$

$$\begin{aligned}
& + \sum_{\alpha \neq \gamma} \sum_{\beta} \left\langle \overset{\circ}{x}_{\alpha}^2 \overset{\circ}{x}_{\gamma}^2 e^{2\pi i(\overset{\circ}{E}_{\alpha} - \overset{\circ}{E}_{\gamma})t} O_{\alpha\beta}^2 O_{\gamma\beta}^2 \right\rangle_{0,V} \\
& = \frac{1}{N(N+2)} \sum_{\beta} \left\langle \sum_{\alpha \neq \gamma} O_{\alpha\beta}^2 O_{\gamma\beta}^2 \left(1 + 2 e^{2\pi i(\overset{\circ}{E}_{\alpha} - \overset{\circ}{E}_{\alpha'})t} \right) + 3 \sum_{\alpha} O_{\alpha\beta}^4 \right\rangle_{0,V}. \quad (37)
\end{aligned}$$

For long times, the time dependence survives only in the picket-fence case. Then, at integer values of t , the fidelity reaches exactly the value of the survival probability. In between, the exponentials give zero on the average. In all other cases, where the spectrum of H_0 is sufficiently random, the exponentials give always zero. To proceed, we will now calculate the limit value of the fidelity (disregarding the exponential). In this case:

$$\begin{aligned}
F_{\infty}^r & = \frac{1}{N(N+2)} \sum_{\xi} \left\langle \sum_{\alpha \neq \beta} O_{\alpha\xi}^2 O_{\beta\xi}^2 + 3 \sum_{\alpha} O_{\alpha\xi}^4 \right\rangle_{0,V} \\
& = \frac{1}{N+2} \left(1 + \frac{2}{N} \sum_{\alpha\xi} \langle O_{\alpha\xi}^4 \rangle_{0,V} \right), \quad (38)
\end{aligned}$$

due to $\sum_{\alpha\beta} O_{\alpha\xi}^2 O_{\beta\xi}^2 = 1$. Hence, both results are linearly related:

$$F_{\infty}^r = \frac{1 + 2 F_{\infty}^e}{N + 2}. \quad (39)$$

Perturbation theory for F_{∞}^e

Here we consider the long time limit F_{∞}^e of the fidelity for initial H_0 -eigenstates, as defined in equation (36). For the GOE case, as well as for the Poisson case, the standard (Rayleigh-Schrödinger) perturbation theory [18] leads to divergences. To obtain meaningful results one had to use degenerate perturbation theory, as in [13]. Unfortunately, this is quite involved in our case, where powers of matrix elements occur up to order four. Therefore we restrict our analytical treatment to the picket-fence case. We assume that the initial state is taken from the centre of the spectrum. As the spectrum is deterministic, only the average over the GOE perturbation matrix V has to be performed. All averages required are of the form $\langle O_{\xi\beta}^2 O_{\mu\beta}^2 \rangle_V$. They are calculated in Appendix B, using the standard perturbation theory. Up to fourth order we obtain:

$$\langle O_{\alpha\alpha}^4 \rangle_V = 1 - 2\lambda^2 \frac{\pi^2}{3} + \lambda^4 \frac{\pi^4}{5} \quad \langle O_{\xi\alpha}^4 \rangle_V = \frac{3\lambda^4}{(\alpha - \xi)^4}, \quad (40)$$

(it is assumed that $\alpha \neq \beta$) and therefore

$$F_{\infty}^e = 1 - 2\lambda^2 \frac{\pi^2}{3} + 4\lambda^4 \frac{\pi^4}{15} + O(\lambda^6). \quad (41)$$

Figure 13 shows F_{∞}^e as a function of the perturbation strength λ for the three different spectral ensembles under consideration. In general the (asymptotic) behaviour of $F_{\infty}^e(\lambda)$ for small λ strongly depends on the degree of level repulsion in the respective spectrum. Our numerical results range from an apparently linear decrease in the Poisson

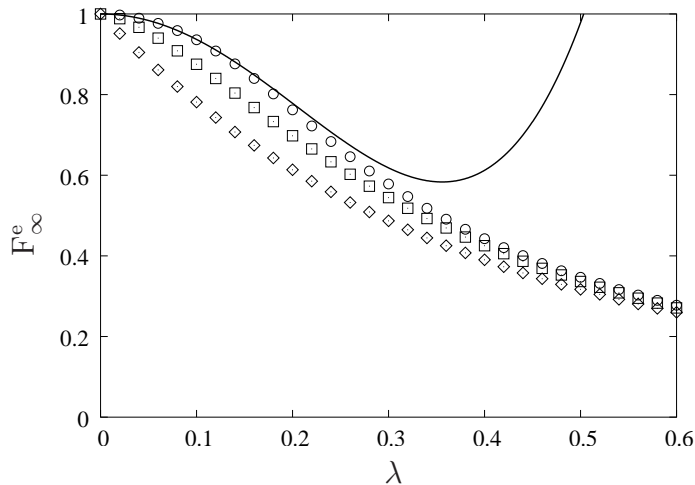


Figure 13. The average fidelity in the large time limit for initial eigenstates of H_0 ($N = 100$). Numerical results for large samples $n_{\text{run}} = 50\,000$, for the Poisson case (\diamond), the GOE (\square), and the picket-fence case (\circ). Perturbation theory, equation (41), for the picket-fence case (solid line).

case up to a quadratic decrease in the picket-fence case, while for the GOE case we obtain some intermediate behaviour. For large λ all curves for $F_\infty^e(\lambda)$ seem to merge into a single one. In the picket-fence case we observe that the perturbative result, equation (41), describes the behaviour at small λ very well.

5. Conclusions

In this paper, we have developed and analysed a random matrix model for echo dynamics in a chaotic system. The fidelity has been computed in the linear response approximation, and a transition from a linear decay to a quadratic one at times of the order of half the Heisenberg time has been found. It is easily verified that in the limit of small perturbations one obtains quite generally a Gaussian decay. By exponentiating our linear response result, we have obtained a theoretical description which reproduces the Gaussian decay in this limit. By construction, this procedure provides a fair approximation for the perturbative and the golden rule regime. However, by comparing with recent fidelity studies for a deterministic chaotic system [13], we could show that our approximation is accurate in the crossover regime also.

The main new ingredient in our approach is the dependence of the fidelity decay on the spectral two-point form factor of the underlying unperturbed Hamiltonian. This lead us to systematically study the effects of spectral correlations on the fidelity decay. Besides the GOE type fluctuations which we expect in classically chaotic systems, we also investigated random spectra (no correlations) and picket-fence spectra (maximal correlations) as the two extreme cases.

In general, we have found that spectral correlations (*i.e.* level repulsion) tend to

inhibit fidelity decay. However, the effect is usually quite small. It becomes big only if we choose eigenstates of the unperturbed Hamiltonian as initial states. Though the correlation effects are really dominant in this case, quantum ergodicity is then lost. This means that the sample-to-sample fluctuations are as large as the fidelity signal itself, so that it is absolutely necessary to perform an ensemble average over many systems, or at least many initial states. In order to restore quantum ergodicity, we need to consider initial states with large IPR's (if expanded in the unperturbed basis). Unfortunately, this inevitably leads to much smaller correlation effects. However, these effects are still observable, even for a single fidelity experiment, provided that the IPR is sufficiently small ($\sim 10^{-3}$).

Finally, we considered the fidelity in the limit of large times. We have shown that the result for a random initial state is related in a simple way to the result for an eigenstate of the unperturbed Hamiltonian. Again we investigated the effect of spectral correlations on this limit value for the fidelity. Using perturbation theory, we could obtain an analytical result for the picket-fence case, valid for small perturbations.

Acknowledgments

We acknowledge useful discussions with W. Strunz and F. Leyvraz. We are grateful to N. Cerruti and S. Tomsovic for providing us with the original data from their standard map calculations (figure 7). This work was supported by the DGAPA (UNAM) grant IN-109000, the CONACyT grant 25192-E, as well as the EU Human Potential Program contract HPRN-CT-2000-00156. TP acknowledges financial support by Ministry of Education, Science and Sports of the Republic of Slovenia, and in part by the US ARO grant DAAD19-02-1-0086.

Appendix A. The correlation integral for different statistical spectra

In order to calculate the correlation integral, equation (14), we need the second integral of the two-point form factor. If we denote the first integral by $B(t)$, we may write:

$$\mathcal{C}(t) = t^2 + \frac{t}{2} - \int_0^t d\tau B(\tau), \quad B(t) = \int_0^t d\tau b_2(\tau). \quad (\text{A.1})$$

For a given statistical spectrum $\{E_\alpha\}$ the two-point form factor $b_2(t)$ is defined in the equations (10) and (11). For the GOE and the GUE case, the two-point form factors are well known [15], and for the Poisson case, $b_2(t)$ is simply zero. Due to the lack of an appropriate reference, we shall calculate $b_2(t)$ for the picket-fence case.

Appendix A.1. Picket-fence

In the picket-fence case, we may assume, that $E_\alpha = \alpha$. With the definition $\xi(t) = \sum_{\gamma=1}^N \exp(2\pi i(\overset{\circ}{E}_\gamma - \overset{\circ}{E}_\alpha) t)$, we may write:

$$\xi(t) = N^{-1} \sum_{\alpha=1}^N q^\alpha \sum_{\beta=1}^N q^{-\beta}, \quad q = e^{2\pi i t}, \quad (\text{A.2})$$

which allows to obtain $\xi(t)$ in closed form. Namely, using the relation $\sum_{\alpha=0}^n q^\alpha = (1 - q^{n+1})/(1 - q)$, we get:

$$\xi(t) = N^{-1} \left(\frac{1 - q^{N+1}}{1 - q} - 1 \right) \left(\frac{1 - q^{-N-1}}{1 - q^{-1}} - 1 \right) = N^{-1} \frac{(1 - q^N)(1 - q^{-N})}{(1 - q)(1 - q^{-1})}, \quad (\text{A.3})$$

so that

$$\xi(t) = N^{-1} \frac{2 - q^N - q^{-N}}{2 - q - q^{-1}} = N^{-1} \frac{1 - \cos(2\pi Nt)}{1 - \cos(2\pi t)} = N^{-1} \frac{\sin^2(\pi Nt)}{\sin^2(\pi t)}. \quad (\text{A.4})$$

Now, we will show that $\xi(t) \rightarrow \sum_{n \in \mathbb{Z}} \delta(t - n)$ in the limit $N \rightarrow \infty$. As $\xi(t)$ is periodic with period one, it is sufficient to consider $t \in (-\frac{1}{2}, \frac{1}{2})$. Let $f(t)$ be an arbitrary smooth function, with support in $(-\frac{1}{2}, \frac{1}{2})$. Then:

$$\begin{aligned} \int dt f(t) \xi(t) &\approx N^{-1} \int_{-N^{-1}}^{N^{-1}} dt f(t) \frac{\sin^2(\pi Nt)}{\sin^2(\pi t)} \approx \frac{f(0)}{N} \int_{-N^{-1}}^{N^{-1}} dt \frac{\sin^2(\pi Nt)}{\pi^2 t^2} \\ &\approx N f(0) \int_{-N^{-1}}^{N^{-1}} dt \cos^2(\pi Nt/2) = \frac{2}{\pi} f(0) \int_{-\pi/2}^{\pi/2} ds \cos^2(s) \approx f(0). \end{aligned} \quad (\text{A.5})$$

This proves the supposition, so that we can conclude:

$$\sum_{n \in \mathbb{Z}} \delta(t - n) = 1 + \delta(t) - b_2(t) \quad \Rightarrow \quad b_2(t) = 1 - \sum_{n \neq 0} \delta(t - n). \quad (\text{A.6})$$

The first and second integral of $b_2(t)$ The first integral of the two-point form factor is:

$$B(t) = \int_0^t d\tau \left[1 - \sum_{n \neq 0} \delta(t - n) \right] = t - [t] \quad [t] = \max_{n \in \mathbb{N}} (n \leq t), \quad (\text{A.7})$$

while for the second integral, we obtain:

$$\int_0^t d\tau B(\tau) = \frac{t^2}{2} - [t] \left(t - \frac{[t] + 1}{2} \right). \quad (\text{A.8})$$

Appendix A.2. GOE case

The two-point form factor for the GOE case reads [15]:

$$\begin{aligned} b_2(t) &= t \ln(2t + 1) - \begin{cases} 2t - 1 & : 0 < t < 1 \\ 1 + t \ln(2t - 1) & : 1 < t \end{cases} \\ &= 1 - 2t + t \ln(2t + 1) + \theta(t - 1) [2(t - 1) - t \ln(2t - 1)], \end{aligned} \quad (\text{A.9})$$

where $\theta(t)$ is the unit step function. Its first integral gives:

$$\begin{aligned}
B(t) &= \int_0^t d\tau b_2(\tau) = t - t^2 + \int_0^t d\tau \tau \ln(2\tau + 1) \\
&\quad + \theta(t-1) \left[\int_0^{t-1} d\tau 2\tau - \int_1^t d\tau \tau \ln(2\tau - 1) \right] \\
&= \frac{5(t-t^2)}{4} + \frac{t^2 - 1/4}{2} \ln(2t + 1) \\
&\quad + \theta(t-1) \left[(t-1)^2 + \frac{(t-1)(t+2)}{4} - \frac{t^2 - 1/4}{2} \ln(2t - 1) \right], \tag{A.10}
\end{aligned}$$

while the second integration yields:

$$\begin{aligned}
\int_0^t d\tau B(\tau) &= \frac{5(t^2/2 - t^3/3)}{4} + \frac{1}{2} \int_0^t d\tau (t^2 - 1/4) \ln(2\tau + 1) + \theta(t-1) \\
&\quad \times \left[\frac{5(t-1)^3}{12} + \frac{3(t-1)^2}{8} - \frac{1}{2} \int_1^t d\tau (t^2 - 1/4) \ln(2\tau - 1) \right]. \tag{A.11}
\end{aligned}$$

The two remaining integrals give:

$$\begin{aligned}
A_1(t) &= \frac{1}{2} \int_0^t d\tau (t^2 - 1/4) \ln(2\tau + 1) = \frac{1}{16} \int_1^{2t+1} ds (s-2)s \ln s \\
&= \frac{1}{16} \left[(y/3 - 1)y^2 \ln y - \frac{y^3 - 1}{9} + \frac{y^2 - 1}{2} \right]_{y=2t+1} \tag{A.12}
\end{aligned}$$

$$\begin{aligned}
A_2(t) &= \frac{1}{2} \int_1^t d\tau (t^2 - 1/4) \ln(2\tau - 1) = \frac{1}{16} \int_1^{2t-1} ds (s+2)s \ln s \\
&= \frac{1}{16} \left[(y/3 + 1)y^2 \ln y - \frac{y^3 - 1}{9} - \frac{y^2 - 1}{2} \right]_{y=2t-1}, \tag{A.13}
\end{aligned}$$

where we have used that:

$$\int_1^y ds s \ln s = \frac{y^2 \ln y}{2} - \frac{y^2 - 1}{4} \quad \int_1^y ds^2 s \ln s = \frac{y^3 \ln y}{3} - \frac{y^3 - 1}{9}. \tag{A.14}$$

Appendix A.3. GUE case

In this case, the two-point form factor is simply:

$$b_2(t) = \begin{cases} 1-t & : 0 < t < 1 \\ 0 & : 1 < t \end{cases}. \tag{A.15}$$

We give the result for the second integral directly:

$$\int_0^t d\tau B(\tau) = \begin{cases} (1-t/3)t^2/2 & : 0 < t < 1 \\ t/2 - 1/6 & : 1 < t \end{cases}. \tag{A.16}$$

Appendix B. Time independent perturbation theory

Consider the Hamiltonian $H = H_0 + \lambda V$. If H_0 has a picket-fence spectrum, we may use the standard (Rayleigh-Schrödinger) perturbation theory to compute low order

approximations to the eigenvectors of H . A compact derivation of the perturbation series can be obtained with the help of the Greens functions for H and H_0 (see reference [18]):

$$G(z) = \frac{1}{z - H}, \quad G_0(z) = \frac{1}{z - H_0} \quad \Rightarrow \quad G(z) = [1 - \lambda G_0(z) V]^{-1} G_0(z). \quad (\text{B.1})$$

Assume that H_0 is diagonal in the basis used: $\langle \alpha | H_0 | \beta \rangle = \delta_{\alpha\beta} \mathring{E}_\alpha$, and define $|e_\alpha\rangle$ as the eigenvector of H , such that:

$$\langle e_\alpha | H | e_\beta \rangle = \delta_{\alpha\beta} E_\alpha \quad |e_\alpha\rangle \rightarrow |\alpha\rangle \quad E_\alpha \rightarrow \mathring{E}_\alpha \quad (\text{B.2})$$

as $\lambda \rightarrow 0$. Then we may write the projector onto the eigenstate $|e_\alpha\rangle$ as follows:

$$P_\alpha = |e_\alpha\rangle \langle e_\alpha| = \frac{1}{2\pi i} \oint dz G(z), \quad (\text{B.3})$$

where the integration path is a simple loop enclosing exclusively the pole \mathring{E}_α of $G_0(z)$ and the pole E_α of $G(z)$. Then we may obtain the perturbation series as follows:

$$P_\alpha^{(n)} = |e_\alpha^{(n)}\rangle \langle e_\alpha^{(n)}| = \sum_{k=0}^n \lambda^k \tilde{T}_\alpha^{(k)}, \quad \tilde{T}_\alpha^{(k)} = \frac{1}{2\pi i} \oint dz [G_0(z) V]^k G_0(z). \quad (\text{B.4})$$

The $\tilde{T}_\alpha^{(k)}$ are operators, and the tilde is used to distinguish them from the matrices $T^{(k)}$ introduced below. Note that so far, the projectors $P_\alpha^{(n)}$ are not normalised, so that an approximation to the absolute value squared of a matrix element of O reads:

$$O_{\xi\alpha}^2 = \frac{\langle \xi | P_\alpha | \xi \rangle}{\sum_\chi \langle \chi | P_\alpha | \chi \rangle} = \frac{\delta_{\xi\alpha} + \sum_{k=1}^n \lambda^k \langle \xi | \tilde{T}_\alpha^{(k)} | \xi \rangle}{1 + \sum_{l=1}^n \lambda^l \sum_{\chi \neq \alpha} \langle \chi | \tilde{T}_\alpha^{(l)} | \chi \rangle} = \frac{\delta_{\xi\alpha} + \sum_{k=1}^n \lambda^k T_{\xi\alpha}^{(k)}}{1 + \sum_{l=1}^n \lambda^l S_\alpha^{(l)}}, \quad (\text{B.5})$$

where $S_\alpha^{(l)} = \sum_{\chi \neq \alpha} T_{\chi\alpha}^{(l)}$. As a final step, one may expand this expression in a Taylor series in λ up to any desired order.

In what follows, we will calculate the matrix elements of O up to forth order in λ and then average the results over the perturbation V which is assumed to be a GOE matrix. To this end, we first consider the operators \tilde{T}_α^k , defined in (B.4):

$$\begin{aligned} \tilde{T}_\alpha^{(0)} &= \frac{1}{2\pi i} \oint dz G_0(z) = |\alpha\rangle \langle \alpha| = p_\alpha \\ \tilde{T}_\alpha^{(1)} &= \frac{1}{2\pi i} \oint dz G_0(z) V G_0(z) = p_\alpha V G'_0 + G'_0 V p_\alpha, \quad G'_0 = \sum_{\beta \neq \alpha} |\beta\rangle \frac{1}{\alpha - \beta} \langle \beta| \\ \tilde{T}_\alpha^{(2)} &= \frac{1}{2\pi i} \oint dz G_0(z) V G_0(z) V G_0(z) \\ &= p_\alpha V G'_0 V G'_0 + G'_0 V p_\alpha V G'_0 + G'_0 V G'_0 V p_\alpha \\ &\vdots \\ \tilde{T}_\alpha^{(n)} &= \sum_{k=0}^n [G'_0 V]^k p_\alpha [V G'_0]^{n-k}. \end{aligned} \quad (\text{B.6})$$

For the matrices $T^{(k)}$, these formulae imply that: $T^{(0)} = 1$, $T^{(1)} = 0$ and $T^{(k)}$ has only zeros on the diagonal for all $k > 1$.

Our aim is it to calculate the average of products of the form $\langle O_{\xi\alpha}^2 O_{\mu\alpha}^2 \rangle_V$. These are in fact just the one-vector averages of order four of this particular ensemble of (approximately) orthogonal matrices. To do so we first expand the squared matrix elements of O in terms of the perturbation parameter λ . Up to fourth order, we get ($\xi \neq \alpha$):

$$O_{\alpha\alpha}^2 = 1 - \sum_{l=2}^4 \lambda^l S_{\alpha}^{(l)} + (\lambda^2 S_{\alpha}^{(2)})^2 = 1 - \lambda^2 S_{\alpha}^{(2)} - \lambda^3 S_{\alpha}^{(3)} - \lambda^4 (S_{\alpha}^{(4)} - S_{\alpha}^{(2)2}) \quad (\text{B.7})$$

$$O_{\xi\alpha}^2 = \sum_{k=2}^4 \lambda^k T_{\xi\alpha}^{(k)} (1 - \lambda^2 S_{\alpha}^{(2)}) = \lambda^2 T_{\xi\alpha}^{(2)} + \lambda^3 T_{\xi\alpha}^{(3)} + \lambda^4 (T_{\xi\alpha}^{(4)} - T_{\xi\alpha}^{(2)} S_{\alpha}^{(2)}) . \quad (\text{B.8})$$

Now, the desired one-vector averages are easily constructed. To this end we assume that the unperturbed energies form the picket-fence spectrum: $\overset{\circ}{E}_{\alpha} = \alpha$, and we consider the limit $N \rightarrow \infty$. Thus, it remains to perform the average over the GOE-matrix V . Henceforth, we use simple angular brackets without subscript to denote such an average. For $\alpha \neq \xi \neq \mu \neq \alpha$, we obtain:

$$\begin{aligned} \langle O_{\alpha\alpha}^4 \rangle &= 1 - 2\lambda^2 \langle S_{\alpha}^{(2)} \rangle - 2\lambda^3 \langle S_{\alpha}^{(3)} \rangle - 2\lambda^4 \left(\langle S_{\alpha}^{(4)} \rangle - \langle S_{\alpha}^{(2)2} \rangle \right) + \lambda^4 \langle S_{\alpha}^{(2)2} \rangle \\ &= 1 - 2\lambda^2 \langle S_{\alpha}^{(2)} \rangle - \lambda^4 \left(2 \langle S_{\alpha}^{(4)} \rangle - 3 \langle S_{\alpha}^{(2)2} \rangle \right) \end{aligned} \quad (\text{B.9})$$

$$\langle O_{\xi\alpha}^4 \rangle = \lambda^4 \langle T_{\xi\alpha}^{(2)2} \rangle \quad (\text{B.10})$$

$$\begin{aligned} \langle O_{\alpha\alpha}^2 O_{\xi\alpha}^2 \rangle &= \left\langle (1 - \lambda^2 S_{\alpha}^{(2)}) \left(\lambda^2 T_{\xi\alpha}^{(2)} + \lambda^3 T_{\xi\alpha}^{(3)} + \lambda^4 [T_{\xi\alpha}^{(4)} - T_{\xi\alpha}^{(2)} S_{\alpha}^{(2)}] \right) \right\rangle \\ &= \lambda^2 \langle T_{\xi\alpha}^{(2)} \rangle + \lambda^4 \left(\langle T_{\xi\alpha}^{(4)} \rangle - 2 \langle T_{\xi\alpha}^{(2)} S_{\alpha}^{(2)} \rangle \right) \end{aligned} \quad (\text{B.11})$$

$$\langle O_{\xi\alpha}^2 O_{\mu\alpha}^2 \rangle = \lambda^4 \langle T_{\xi\alpha}^{(2)} T_{\mu\alpha}^{(2)} \rangle . \quad (\text{B.12})$$

There are in total eight different quantities to average:

$$\langle T_{\xi\alpha}^{(2)} \rangle = \left\langle \frac{1}{\alpha - \xi} V_{\xi\alpha} V_{\alpha\xi} \frac{1}{\alpha - \xi} \right\rangle = \frac{1}{(\alpha - \xi)^2} \quad (\text{B.13})$$

$$\langle S_{\alpha}^{(2)} \rangle = \sum_{\xi \neq \alpha} \langle T_{\xi\alpha}^{(2)} \rangle = \frac{\pi^2}{3} \quad (\text{B.14})$$

$$\langle T_{\xi\alpha}^{(2)2} \rangle = \left\langle \left(\frac{V_{\xi\alpha}^2}{(\alpha - \xi)^2} \right)^2 \right\rangle = \frac{3}{(\alpha - \xi)^4} \quad (\text{B.15})$$

$$\langle T_{\xi\alpha}^{(2)} T_{\mu\alpha}^{(2)} \rangle = \left\langle \frac{V_{\xi\alpha}^2}{(\alpha - \xi)^2} \frac{V_{\mu\alpha}^2}{(\alpha - \mu)^2} \right\rangle = \frac{1}{(\alpha - \xi)^2 (\alpha - \mu)^2} \quad (\text{B.16})$$

$$\begin{aligned} \langle S_{\alpha}^{(2)2} \rangle &= \sum_{\{\xi \neq \mu\} \neq \alpha} \langle T_{\xi\alpha}^{(2)} T_{\mu\alpha}^{(2)} \rangle + \sum_{\xi \neq \alpha} \langle T_{\xi\alpha}^{(2)2} \rangle \\ &= \sum_{\{\xi \neq \mu\} \neq \alpha} \frac{1}{(\alpha - \xi)^2 (\alpha - \mu)^2} + \sum_{\xi \neq \alpha} \frac{3}{(\alpha - \xi)^4} \\ &= \left(\sum_{\xi \neq \alpha} \frac{1}{(\alpha - \xi)^2} \right)^2 + \sum_{\xi \neq \alpha} \frac{2}{(\alpha - \xi)^4} = \frac{7 \pi^4}{45} \end{aligned} \quad (\text{B.17})$$

$$\begin{aligned}
\langle T_{\xi\alpha}^{(4)} \rangle &= \sum_{\mu, \nu \neq \alpha} \left\{ \left\langle \frac{1}{\alpha - \xi} V_{\xi\alpha} V_{\alpha\mu} \frac{1}{\alpha - \mu} V_{\mu\nu} \frac{1}{\alpha - \nu} V_{\nu\xi} \frac{1}{\alpha - \xi} \right\rangle \right. \\
&\quad + \left\langle \frac{1}{\alpha - \xi} V_{\xi\mu} \frac{1}{\alpha - \mu} V_{\mu\alpha} V_{\alpha\nu} \frac{1}{\alpha - \nu} V_{\nu\xi} \frac{1}{\alpha - \xi} \right\rangle \\
&\quad \left. + \left\langle \frac{1}{\alpha - \xi} V_{\xi\mu} \frac{1}{\alpha - \mu} V_{\mu\nu} \frac{1}{\alpha - \nu} V_{\nu\alpha} V_{\alpha\xi} \frac{1}{\alpha - \xi} \right\rangle \right\} \\
&= \frac{1}{(\alpha - \xi)^2} \left\{ \sum_{\nu \neq \alpha} \frac{\langle V_{\xi\alpha}^2 V_{\xi\nu}^2 \rangle}{(\alpha - \xi)(\alpha - \nu)} + \sum_{\mu \neq \alpha} \frac{\langle V_{\xi\mu}^2 V_{\mu\alpha}^2 \rangle}{(\alpha - \mu)^2} + \sum_{\mu \neq \alpha} \frac{\langle V_{\xi\mu}^2 V_{\xi\alpha}^2 \rangle}{(\alpha - \mu)(\alpha - \xi)} \right\} \\
&= \frac{1}{(\alpha - \xi)^4} + \frac{\pi^2}{3} \frac{1}{(\alpha - \xi)^2} \tag{B.18}
\end{aligned}$$

$$\langle S_{\alpha}^{(4)} \rangle = \sum_{\xi \neq \alpha} \langle T_{\xi\alpha}^{(4)} \rangle = \frac{\pi^4}{45} + \frac{\pi^4}{9} = \frac{2\pi^4}{15} \tag{B.19}$$

$$\begin{aligned}
\langle S_{\alpha}^{(2)} T_{\xi\alpha}^{(2)} \rangle &= \langle T_{\xi\alpha}^{(2)2} \rangle + \sum_{\mu \neq \xi, \alpha} \langle T_{\xi\alpha}^{(2)} T_{\mu\alpha}^{(2)} \rangle = \frac{3}{(\alpha - \xi)^4} + \sum_{\mu \neq \xi, \alpha} \frac{1}{(\alpha - \xi)^2 (\alpha - \mu)^2} \\
&= \frac{2}{(\alpha - \xi)^4} + \frac{\pi^2}{3} \frac{1}{(\alpha - \xi)^2}. \tag{B.20}
\end{aligned}$$

References

- [1] Loschmidt J (ca. 1870) Private communication to L. Boltzmann
Cercignani C (1970) *Ludwig Boltzmann: The man who trusted Atoms* (New York: University Press)
- [2] Hahn E L (1950) *Phys. Rev.* **80** 580-94
Rhim W-K, Pines A and Waugh J S (1970) *Phys. Rev. Lett.* **25** 218-20
Brewer R G and Hahn E L (1984) *Sci. Am.* **251**(6) 42-5
Zhang S, Meier B H and Ernst R R (1992) *Phys. Rev. Lett.* **69** 2149-51
Pastawski H M, Levstein P R and Usaj G (1995) *Phys. Rev. Lett.* **75** 4310-13
Levstein P R and Usaj G (1998) *J. Chem. Phys.* **108** 2718-24
Usaj G, Pastawski H M and Levstein P R (1998) *Mol. Phys.* **95** 1229-36
Zhang W and Cory D G (1998) *Phys. Rev. Lett.* **80** 1324-27
Pastawski H M, Levstein P R and Usaj G (2000) *Physica A* **283** 166-70
- [3] Peres A (1984) *Phys. Rev. A* **30** 1610-15
- [4] Prosen T and Žnidarič M (2002) *J. Phys. A: Math. Gen.* **35** 1455-81
- [5] Kaplan L (2002) *New J. Phys.* **4** 90
- [6] Jalabert R A and Pastawski H M (2001) *Phys. Rev. Lett.* **86** 2490-93
- [7] Jacquod P, Silvestrov P G and Beenakker C W J (2001) *Phys. Rev. E* **64** 055203(R)
- [8] Cerruti N R and Tomsovic S (2002) *Phys. Rev. Lett.* **88** 054103
- [9] Prosen T, Seligman T H and Žnidarič M (2003) *Prog. Theo. Phys. Supp.* **150** 200-28
- [10] Cohen D (2000) *Ann. Phys. (N.Y.)* **283** 175-231
- [11] Casati G, Valz-Gris F and Guarneri I (1980) *Lett. Nuovo Cimento* **28** 279-82
Bohigas O, Giannoni M J and Schmit C (1984) *Phys. Rev. Lett.* **52** 1-4
Berry M V (1985) *Proc. R. Soc. Lond. A* **400** 229-51
Leyvraz F and Seligman T H (1992) *Phys. Lett. A* **168** 348-52
Andreev A V, Agam O, Simons B D and Altshuler B L (1996) *Phys. Rev. Lett.* **76** 3947-50
- [12] Berry M V and M. Tabor M (1977) *Proc. R. Soc. Lond. A* **356** 375-94

- [13] Cerruti N R and Tomsovic S (2003) *J. Phys. A: Math. Gen.* **36** 3451–65
Cerruti N R and Tomsovic S (2003) *J. Phys. A: Math. Gen.* **36** 11915–16
- [14] Prosen T and Žnidarič M (2001) *J. Phys. A: Math. Gen.* **34** L681-87
- [15] Mehta M L (1991) *Random Matrices and the Statistical Theory of Energy Levels* (New York: Academic Press)
- [16] Leviandier L, Lombardi M, Jost R, and Pique J P (1986) *Phys. Rev. Lett.* **56** 2449-52
- [17] Prosen T and Seligman T H (2002) *J. Phys. A: Math. Gen.* **35** 4707-27
Tanaka A, Fujisaki H and Miyadera T (2002) *Phys. Rev. E* **66** 045201(R)
Žnidarič M and Prosen T (2003) *J. Phys. A: Math. Gen.* **36** 2463-81
- [18] Messiah A (1979) *Quantenmechanik, Bd. 2* (New York: Walter de Gruyter)